Thermal Property Estimation of Fibrous Insulation: Heat Transfer Modeling and the Continuous Genetic Algorithm

Elora Frye[1]
NASA Langley Research Center, Hampton, VA, 23681, USA

Kamran Daryabeigi[2]
NASA Langley Research Center, Hampton, VA, 23681, USA

Thermal properties of high-temperature fibrous insulation materials were estimated from transient thermal tests using an inverse heat transfer technique. Transient temperature data from an experimental set up was collected and a simple, one-dimensional numerical model was constructed to replicate the temperatures within the test assembly. The Continuous Genetic Algorithm optimization technique in conjunction with a numerical thermal model and transient test data was used to estimate coefficients of a functional representation of the thermal property. The thermal properties, i.e., thermal conductivity and specific heat, of an alumina insulation felt were estimated over the temperature range of 300 K to 1700 K at various constant static pressures in nitrogen gas and compared with published data. The resulting thermal property estimates were within 10% of published values over the entire temperature range at various pressures. The methodology, application, and results are presented.

I. Nomenclature

$\boldsymbol{A}$ = collected temperature vector from experimental test assembly
b_j = coefficients of the functional representation of specific heat at constant pressure, $j \in \{0,1\}$
c_j = coefficients of the functional representation of thermal conductivity, $j \in \{0,1,2,3\}$
c_p = specific heat at constant pressure, *J/kg/K*
i = time index
k = thermal conductivity, *W/m/K*
m = number of times steps
r_x = relative temperature difference at location *x*
R = total relative difference
t = time, *sec*
T = measured temperature, *K*
ΔT_j = absolute temperature difference of numerical solution and experimental data at TC location $A_j, j \in \{2,4,6,8\}$
u = analytical temperature, *K*
$\hat{u}$ = numerical model temperature approximation, *K*
x = location, *m*
z = objective function value
ρ = density, kg/m^3

II. Introduction

Thermal protection systems (TPS) protect space flight vehicles from the large thermal loads experienced during entry into a planet's atmosphere. The thermal properties, thermal conductivity and specific heat, of TPS materials, such as light-weight insulations, are essential to reliably predict performance of the system during flight. The purpose of this work was to estimate the material thermal properties, thermal conductivity and specific heat, of high-

[1] Research Engineer, Structural Mechanics and Concepts Branch, MS 190.
[2] Senior Research Engineer, Structural Mechanics and Concepts Branch, MS 190.

temperature fibrous insulation materials based on data from transient thermal tests in conjunction with the Continuous Genetic Algorithm (CGA) optimization technique.

Over the years, many techniques have been investigated to estimate the thermal properties of high-porosity, low-density thermal insulation materials. Standard measurement techniques include steady-state methods to estimate thermal conductivity [1, 2, 3] and a standard method for specific heat [4]. The steady-state techniques require significant test time to achieve the steady-state conditions needed to yield accurate results. Other techniques include optimization methods that have been used in conjunction with experimental test data and a numerical heat transfer model to estimate thermal properties. Common optimization techniques include gradient based, statistical, and genetic algorithm (GA) methods. A commonly used gradient based technique is the conjugate gradient method as used by Alifanov and Mikhailov to solve an inverse heat transfer problem [5]. A Gauss minimization method, which does require the computation of gradients, was used by Scott and Beck [6] with transient temperature data to estimate thermal properties of composite materials. Williams and Curry [7] applied a least squares technique, which does not require the calculation of gradients, to transient experimental data to estimate the thermal properties of fibrous insulation materials. GA methods have been applied to heat transfer problems such as the optimization of experimental design, estimation of surface heat fluxes, and estimation of thermal properties. Many of the applications in the literature are summarized by Gosselin et al. [8]. The advantages of GAs over gradient based methods include no need to compute the gradient of the objective function, the algorithms are likely not to converge to a local minima, and the solution is less sensitive to the initial guess [8]. Thermal properties have been estimated using GAs in combination with transient and steady-state experiments. Daryabeigi applied a GA with steady-state temperature data to predict specific extinction coefficients needed for effective radiant thermal conductivity [3]. The use of transient temperature data with GA has been developed for estimating thermal properties and used in other applications such as complex aerospace structures [9, 10].

In the work presented, thermal properties of alumina paper (APA) fibrous insulation were estimated using transient temperature data and the CGA. A continuous algorithm was chosen as the values estimated are floating point numbers. First, temperature data was collected through thermal vacuum chamber tests of the insulation material. Then, a finite difference numerical model was developed to predict the heat transfer through the materials in the test setup. The CGA was used to determine a functional representation of the thermal properties by minimizing the difference between measured and numerical model predicted temperatures at various through-thickness locations in the insulation. The algorithm searched the parameter space for coefficients of a functional representation of the thermal property, that when used in the numerical model minimizes the difference between the experimental temperature data and the numerical model values. In high porosity insulation, typically larger than 90 percent, the thermal conductivity is a function of the environmental pressure and gaseous medium in addition to the temperature [3]. Therefore the method was applied to transient temperature data at various pressures. The results of estimating the thermal properties of APA over the temperature range of 300 K to 1700 K at constant static pressures of 13.33 kPa, 1.33 kPa, and 13.33 Pa in nitrogen gas are compared to published data [3,11] and discussed.

III. Thermal Testing

Temperature data was collected from a transient thermal testing facility located at NASA Langley Research Center in Hampton, Virginia. The test assembly, shown in Fig. 1, was contained in a thermal vacuum chamber to allow control of the pressure during testing. The graphite heater was used to control the temperature on the top surface of the test assembly. The major components of the test assembly were 305mm by 305mm wide and were surrounded by rigid insulation boards to minimize lateral heat losses.

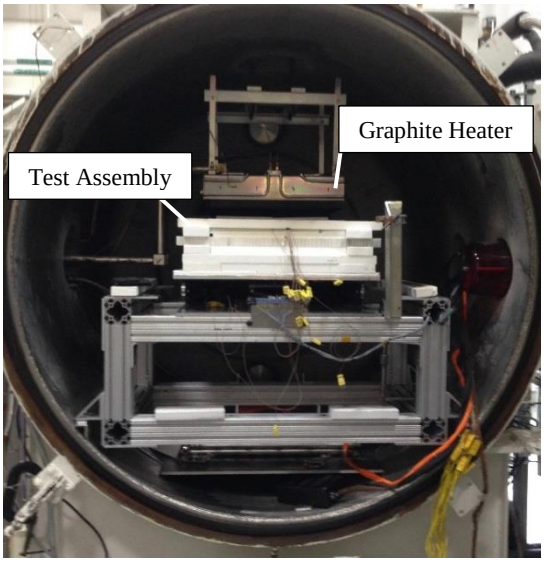

Figure 1. The graphite heater and test assembly shown in thermal vacuum chamber.

Components of the test assembly are shown in Fig. 2. A 4.3 mm thick composite plate made of Advanced Carbon-Carbon 6 (ACC-6) was placed below the heater to evenly distribute the heat into the sample. There were eight surface mounted thermocouples (TCs) installed on the ACC-6 plate, four on the top and four on the bottom. Ten layers of the fibrous insulation, APA, with an effective thickness of 12.7 mm were placed below the ACC-6 plate. Four TCs were placed within the APA layers at depths of 2.54 mm, 5.08 mm, 7.62 mm, and 10.16 mm below the ACC-6 plate. A 2.5 mm thick titanium (Ti) plate was placed below the APA layers with eight TCs spot welded on the bottom of the plate. There was a 25.4 mm thick air gap below the Ti plate, then a 50.8mm thick aluminum plate that acted as a heat sink. More details about the test assembly are given in [12]. The experiments were conducted at constant static pressures of 13.33 kPa, 1.33 kPa, and 13.33 Pa in nitrogen gas and temperature data was collected at 1 Hz.

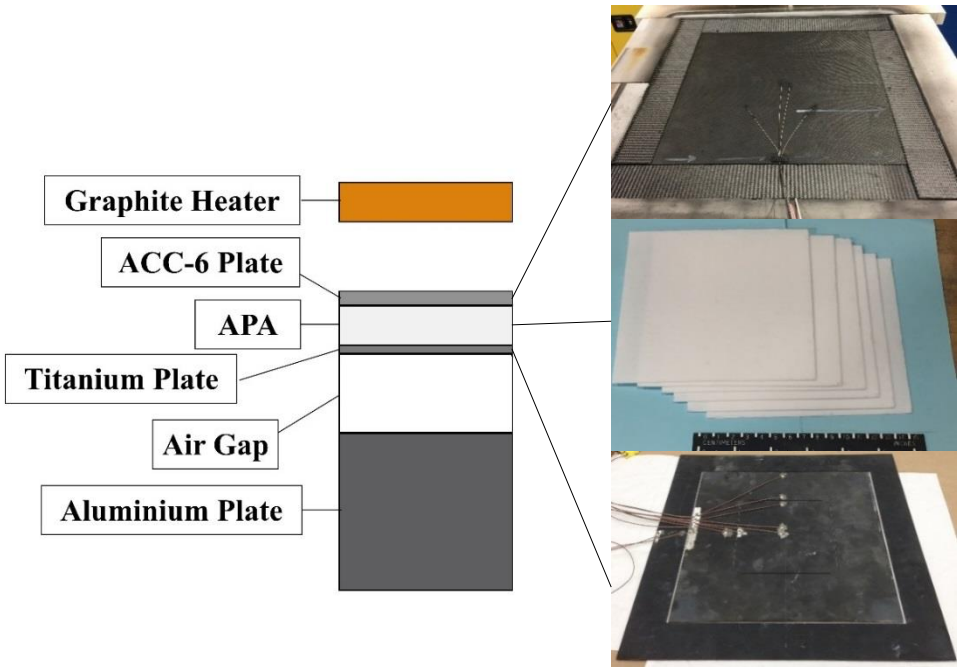

Figure 2. Diagram of test assembly (not to scale) and components.

IV. Thermal Modeling

The temperatures within the experimental apparatus were estimated by a numerical solution of the one-dimensional heat conduction partial differential equation subject to the boundary and initial conditions defined as

$$\begin{aligned} \frac{\partial}{\partial x}\left(k(u)\frac{\partial u}{\partial x}\right) &= \rho c_p(u)\frac{\partial u}{\partial t}, && 0 < x < L \\ u(x,0) &= f(x), && 0 \le x \le L \\ u(0,t) &= g(t), && 0 < t \\ u(L,t) &= h(t), && 0 < t. \end{aligned} \tag{1}$$

An energy balance method was used to construct a finite-difference approximation of the temperatures within the apparatus. The Crank-Nicolson scheme was used for time marching [14], and the resulting tridiagonal systems of equations at each time step were solved using the Thomas Algorithm [15]. The analytical temperature solution, *u*, was approximated by the finite-difference method, $\hat{u}$, for spatial location *x* at time *t*. The domain modeled was from the bottom of the ACC-6 plate, x=0, to the bottom of the Ti plate, x = L, with L = 15.24 as shown in Fig. 3. Certain nodes correspond to TC locations within the test assembly. The TC locations within the APA are referenced as A_2, A_4, A_6, and A_8; where the subscript denotes the location with respect to felt layer number measured from the bottom layer. For example, temperature data collected from location A_4 was on top of the fourth layer of APA when counting from the bottom layer.

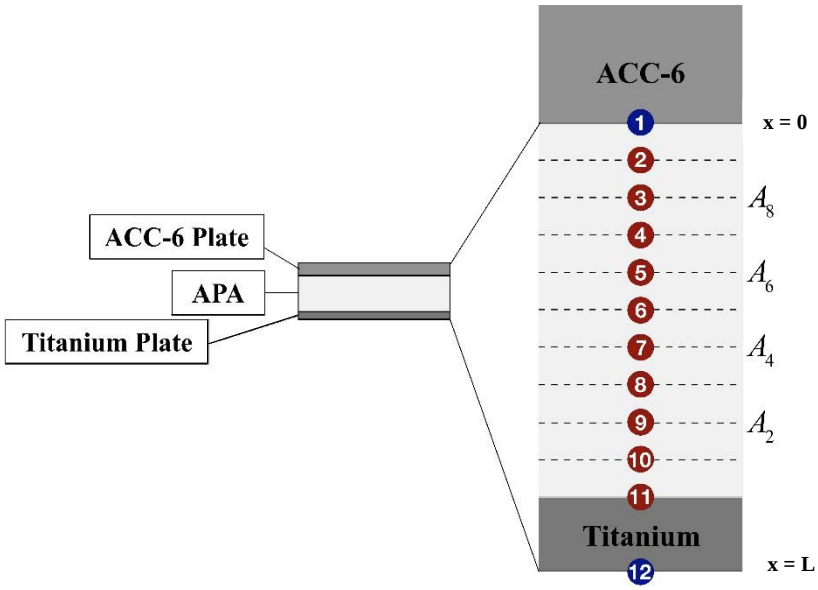

Figure 3. Diagram of test assembly components (not to scale) and numerical model domain with nodal and TC locations.

Experimental temperature data were used as the initial condition and Dirichlet boundary conditions. The initial condition, *f*(*x*), was interpolated from the initial temperature data throughout the domain. The hot side boundary condition, *g*(*t*) at node 1 in Fig. 3, was an average of two center TCs from the bottom of the ACC-6 plate. The other central TCs on the plate were not included in the average as they occasionally malfunctioned. The cold side boundary condition, *h*(*t*) at node 12 in Fig. 3, was an average of four central TCs on the bottom of the Ti plate. A time step of one second was used to match the experimental data acquisition rate.

A grid convergence study was performed to determine the appropriate number of nodes in the model for accuracy and efficiency. The 12-node model, $\hat{u}_1$, had a node at each material interface, shown in Fig. 3. A 22-node model, $\hat{u}_2$, was generated from the 12-node model by adding a node in the center of each layer of APA. Each model was solved with the initial and boundary conditions from the experimental test data. A cubic fit to published data was used as the thermal conductivity, *k*, of APA [3]. An exponential fit to published data was used as the specific heat, c_p, of APA [11]. The thermal properties for the Ti plate were interpolated functions from test data produced by a commercial thermal property measurement laboratory [13]. The temperature results from each model were compared for the common nodal locations using an absolute relative difference, r_x, defined at location *x* as

$$r_x(\hat{u}_1, \hat{u}_2) = \frac{|\hat{u}_1(x) - \hat{u}_2(x)|}{\hat{u}_2(x)} \ . \tag{2}$$

The results for the four locations corresponding to the APA TCs are shown in Fig. 4.

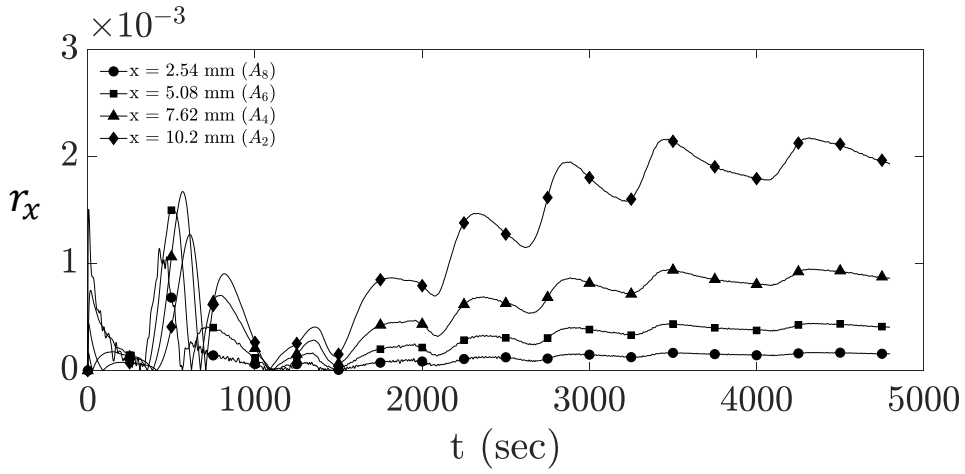

Figure 4. Absolute relative difference between the 12 node model and 22 node model at four locations throughout the domain.

The maximum relative difference of the four TC locations was less than 0.25%. The total relative difference, defined as

$$R = \sum_{i=1}^{10} r_{x_i} \ , \tag{3}$$

was calculated at each time step. The results are shown in Fig. 5. The total relative difference over all 10 common nodal locations for each time step was below 1%. Thus, adding nodes between material interfaces did not significantly improve the solution accuracy and increased the computation time by a factor of four. Therefore the 12-node model was used in the estimation of the thermal properties.

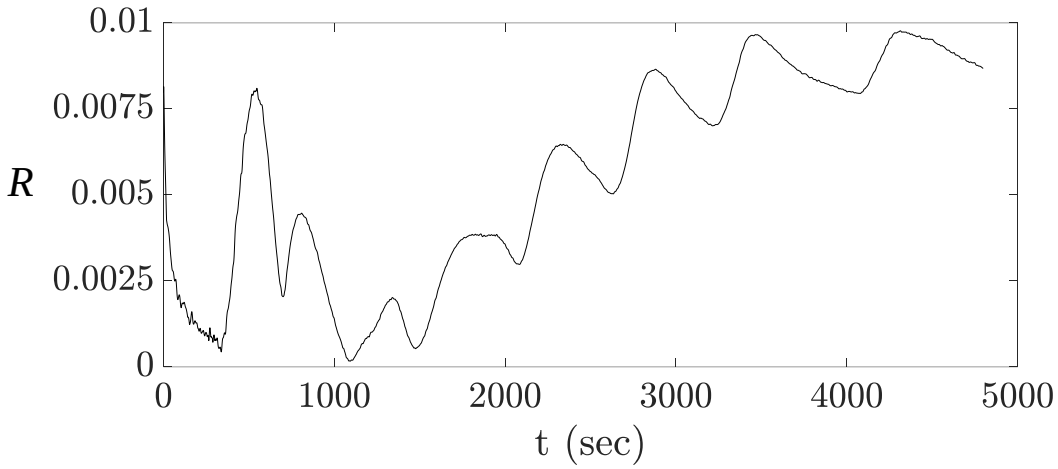

Figure 5. Total absolute relative difference for all 10 common nodal locations.

V. Thermal Property Estimation

The inverse heat transfer problem of estimating thermal material properties typically involves minimizing the difference between measured and computed temperatures. Common optimization techniques used to estimate thermal properties include gradient descent, conjugate gradient, and GA. One possible advantage of GA over other optimization techniques is the ability to locate the global minimum of an objective function that has many local minima. In this work, the CGA optimization technique was chosen to estimate thermal conductivity and specific heat as functions of temperature. The parameters needed are floating point numbers, therefore a continuous algorithm was used instead of a binary algorithm. The goal was to determine the coefficients of the functional representation of the thermal properties that minimize the difference between the measured and predicted temperature values at a single location within the APA. The functional representation of thermal conductivity for the highly porous APA was assumed to be a third order polynomial function of temperature [3]

$$k(u) = c_0 + c_1 u + c_2 u^2 + c_3 u^3, \tag{4}$$

which is an effective thermal conductivity that combines contributions of various modes of heat transfer in fibrous insulation (gas conduction, solid conduction, and radiation). The coefficients c_0, c_1, c_2, and c_3 were assumed to be within the specific intervals

$$\begin{aligned} c_0 &\in [-10^{-2}, 10^{-2}] \\ c_1 &\in [-10^{-3}, 10^{-3}] \\ c_2 &\in [-10^{-6}, 10^{-6}] \\ c_3 &\in [-10^{-10}, 10^{-10}]. \end{aligned}$$

The functional representation of specific heat for APA was assumed to be a bounded exponential [11] defined as

$$c_p(u) = b_0\left(1 - \frac{1}{e^{b_1 u}}\right), \tag{5}$$

where b_0 is the upper bound and b_1 is the growth rate. The coefficients were assumed to be in defined intervals based on prior knowledge of specific heat values for various fibrous insulations [11]

$$\begin{aligned} b_0 &\in [800,1400] \\ b_1 &\in [0, 10^{-2}]. \end{aligned}$$

The coefficients are estimated by searching the parameter space for the set that best minimizes the objective function, *z*, given by

$$z(\hat{\boldsymbol{u}}) = \sum_{i=1}^{m} \left(\frac{A(i) - \hat{u}(i)}{A(i)} \right)^2, \tag{6}$$

where $\boldsymbol{A}$ is a vector of measured temperatures from one TC location within the APA (A_2, A_4, A_6, or A_8), $\hat{\boldsymbol{u}}$ is a vector of predicted temperatures at the corresponding nodal location within the numerical model, and m is the number of time steps.

The coefficient space is searched using the CGA to find the set of coefficients that, when used as the coefficients of the functional representation of the thermal property in the numerical model, minimizes Eq. 6. CGA has many forms and the details can be found in [16]. The procedure used in this work is summarized in Fig. 6. More details on the application of CGA to the estimation of thermal properties can be found in [17].

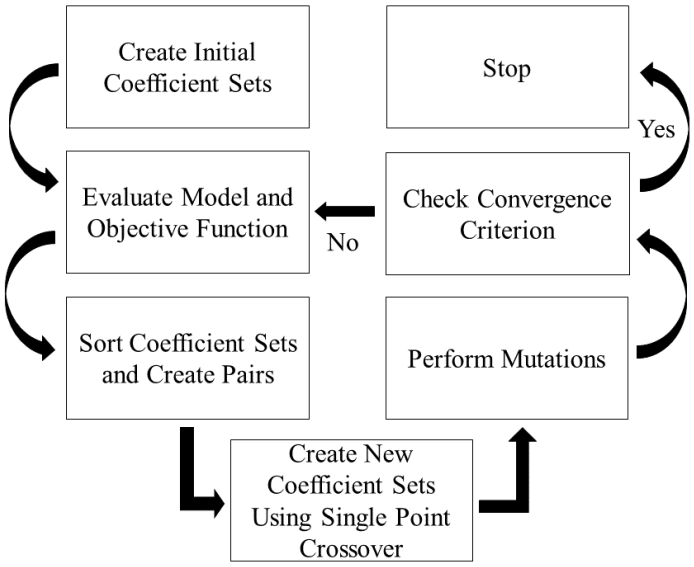

Figure 6. The CGA for estimation of thermal properties

CGA begins by constructing the initial population containing sets of coefficients for the functional representation of the thermal property. The CGA samples a uniform distribution defined on the intervals given for each coefficient to construct the initial coefficient sets. The sets are then used individually as the coefficients of the functional representation for the thermal property of APA in the numerical model. The objective function, Eq. 6, is evaluated using the predicted temperatures for each coefficient set. The resulting z-values from each set of coefficients are sorted from smallest to largest, creating a list with the most successful coefficient sets at the top and the least successful on the bottom. The algorithm then selects the top 50% of the population and randomly pairs sets together to create new coefficient sets by performing single point crossover as shown in Fig. 7. A single dividing point is chosen at random and the coefficients to the right of the point are swapped.

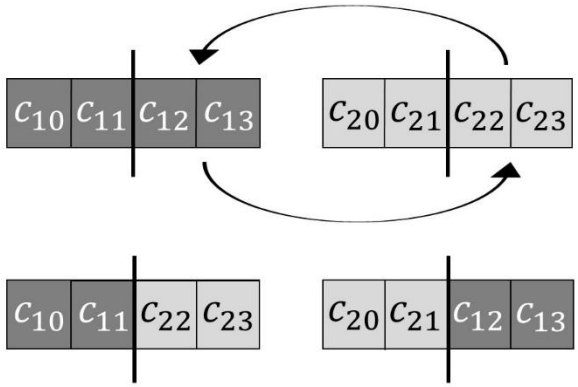

Figure 7. Example of single point crossover.

The new sets of coefficients are combined with the original top 50% of the population to create the new population. Then, a percentage of the new population is mutated to add variety to the possible solutions. The mutations are performed by randomly selecting a percentage of individual coefficients and replacing each coefficient with a value within the given intervals. The mutations allow the algorithm to search in other areas of the parameter space and shift out of possible local minima. The process continues until one of two stopping criteria are met. The algorithm terminates if the maximum number of iterations has been met or if the z-value is below the specified threshold. If neither condition is met, the algorithm continues on for another iteration by evaluating the model and objective function for the new population. The result is a set of coefficients that minimize the objective function within the allotted number of iterations.

VI. Results for Thermal Property Estimation

The thermal properties of APA were estimated using experimental temperature data, the numerical model constructed to estimate the temperatures within the experimental apparatus, and the CGA optimization technique. The algorithm searched the parameter space for the coefficients of the functional representation of the thermal property that minimize the difference between the experimental data and numerical approximation at one particular TC location. The thermal properties were estimated for each TC location individually to determine the depth that provides the most accurate estimates compared to the published values [3]. Thermal conductivity and specific heat were estimated independently. When k was approximated, c_p was assumed to be known and modeled as a bounded exponential fit to theoretical data for alumina [11]. When c_p was estimated, k was assumed to be known and modeled as a cubic fit to published data [3]. The method was applied to experimental data at 13.3 kPa, 1.33 kPa, and 13.3 Pa to determine the variation of thermal conductivity with pressure. The temperature profile for each test has multiple ramps and dwells as the tests were originally performed to estimate properties of the ACC-6 plate from the quasi-steady-state portions of the data. The existing test data was used to evaluate the methodology discussed when applied to APA.

A temperature profile, table, and graph of thermal property results corresponding to the estimated coefficients are given for each set of results at the specified pressure. In the temperature profiles presented, the top black line was an average of the two center TCs on the bottom of the ACC-6 plate, and the bottom gray line was an average of the four center TCs on the Ti plate. The specified temperatures were used as the hot and cold side boundary conditions, respectively. Temperature data at the four TC locations within the insulation are shown in each temperature profile with various shape markers to identify the separate locations. The convergence criteria used for the CGA was a maximum number of iterations of 300 and a threshold value of 0.01. The algorithm commonly terminated because the maximum number of iterations was met. The coefficient ranges were perturbed if any of the solutions were on the boundary of their intervals when the maximum number of iterations were met. Thermal conductivity results at each location for each test and specific heat results for one test are presented.

A. 13.3 kPa Thermal Conductivity Results

The temperature profile of the test conducted at 13.3 kPa is given in Fig. 8. The test had a minimum temperature of 300 K and a maximum temperature of approximately 1250 K with three ramps and dwells. During the test, TC A_4 malfunctioned and was not included in the analysis. The thermal conductivity was approximated between 300 K and 1400 K.

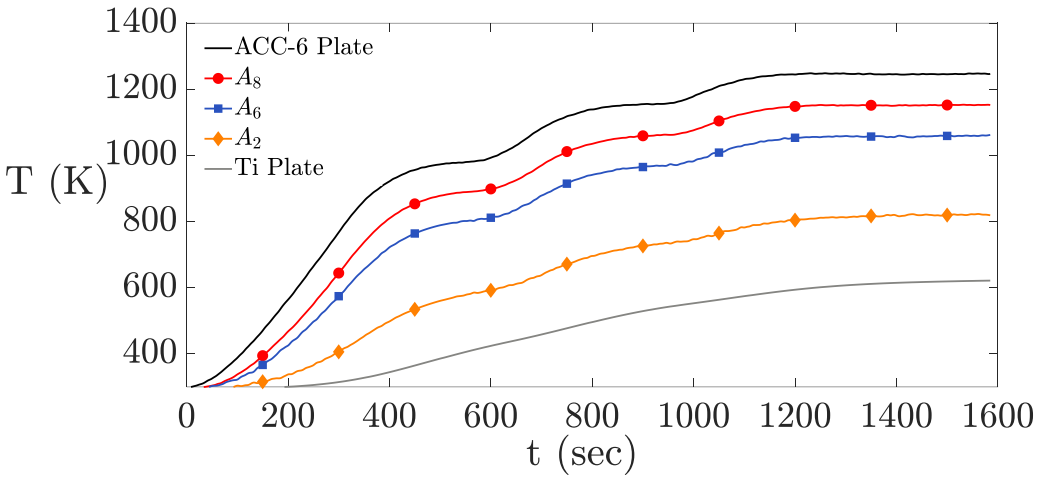

Figure 8. Temperature data collected from the experimental apparatus at 13.3 kPa.

The coefficients of the thermal conductivity function in Eq. 4 were estimated for each TC location. The results from each location are given in Table 1, which includes the coefficients and corresponding objective function value. TC location A_2, which was farthest away from the heat source, produced the lowest *z*-value and which corresponded to the smallest temperature difference between the computed and collected temperatures at that particular location. TC location A_8, which was closest to the heat source, presented the second lowest *z*-value.

Table 1. Thermal conductivity coefficients and associated objective function values for each TC location at 13.3 kPa.

TC Location	z	c_0	c_1	c_2	c_3
A_8	0.026	$5.98 \cdot 10^{-5}$	$4.99 \cdot 10^{-5}$	$-8.50 \cdot 10^{-9}$	$9.92 \cdot 10^{-12}$
A_6	0.077	$7.31 \cdot 10^{-8}$	$9.06 \cdot 10^{-5}$	$-3.73 \cdot 10^{-11}$	$9.96 \cdot 10^{-12}$
A_2	0.023	$1.17 \cdot 10^{-5}$	$1.01 \cdot 10^{-4}$	$-5.89 \cdot 10^{-8}$	$8.03 \cdot 10^{-11}$

The associated thermal conductivity functions are compared with the published values [3] in Fig. 9. The result from the A_2 TC location was the best estimate compared to the published thermal conductivity values. It was not expected that the TCs farthest away from the heat source would provide estimates with the smallest percent difference compared to the published values. Estimates obtained from TCs closer to the heated surface under predict the thermal conductivity. For the solution corresponding to A_2, there was an average relative difference of 7.29% with respect to published data over the entire temperature range. Above 800 K, the average relative difference was 2.72%. Note that TC location A_8 produced the second smallest *z*-value but when compared to the published values, that location had the largest difference. The results indicate that small z-values do not imply close approximations compared to the published values. The issue is discussed in section VII.

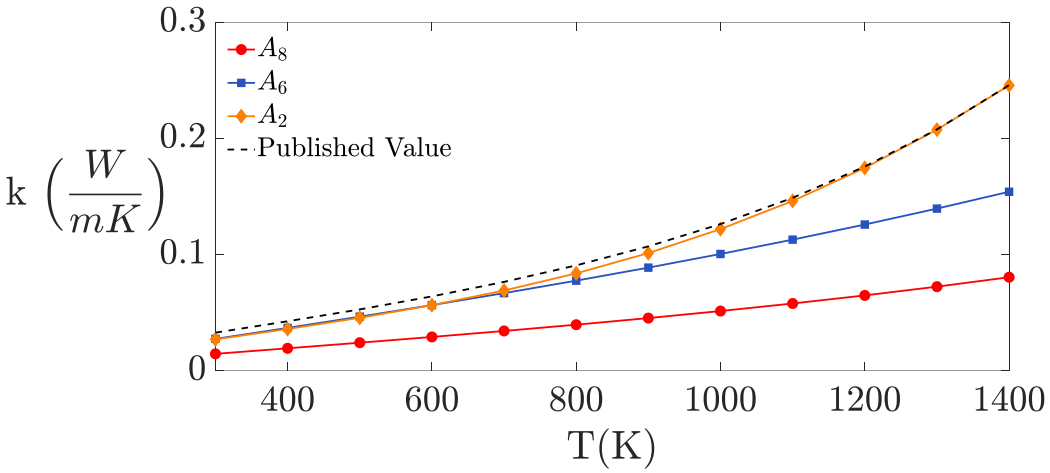

Figure 9. Thermal conductivity estimates from each TC location compared with published values at 13.3 kPa.

B. 1.33 kPa Thermal Conductivity Results

The 1.33 kPa temperature profile is given in Fig. 10. For this test, the temperature of the ACC-6 plate begins at approximately 600 K. The data acquisition system malfunctioned and temperature data was not collected until after the thermal load was initiated. The temperature data recorded after the malfunction is presented and used for the analysis. The test had a minimum temperature of 400 K and a maximum temperature of approximately 1550 K and consisted of five ramps and dwells.

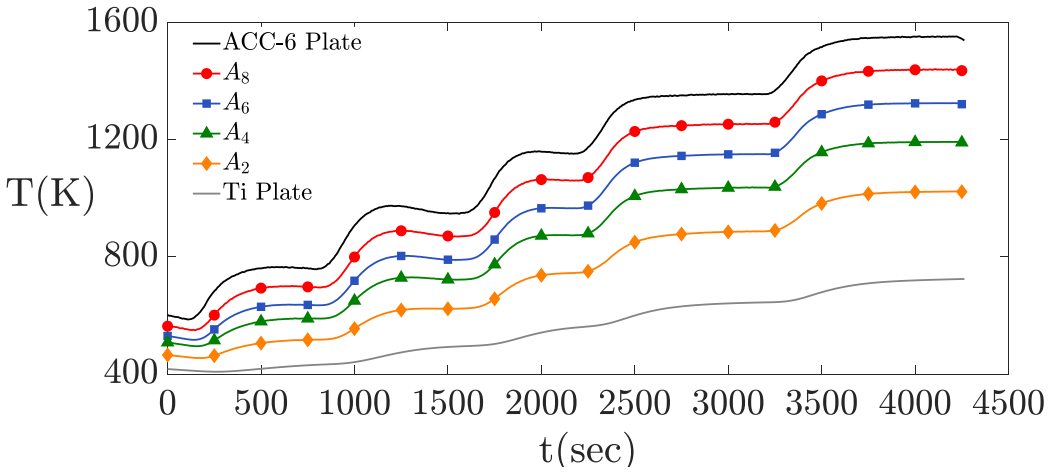

Figure 10. Temperature data collected from experimental apparatus at 1.33 kPa.

The estimated coefficients for the thermal conductivity functional representation, Eq. 4, with the lowest z-value at each TC location are provided in Table 2. TC location A_2 produced the lowest *z*-value. The other TC locations A_8, A_6, and A_4 produced increasingly larger z-values, respectively.

Table 2. Thermal conductivity coefficients and associated objective function values for each TC location at 1.33 kPa.

TC Location	z	c_0	c_1	c_2	c_3
A_8	0.067	$2.50 \cdot 10^{-2}$	$1.54 \cdot 10^{-6}$	$-1.47 \cdot 10^{-9}$	$1.70 \cdot 10^{-11}$
A_6	0.054	$3.73 \cdot 10^{-2}$	$1.93 \cdot 10^{-7}$	$-2.00 \cdot 10^{-9}$	$3.51 \cdot 10^{-11}$
A_4	0.021	$-8.42 \cdot 10^{-3}$	$1.15 \cdot 10^{-4}$	$-8.42 \cdot 10^{-8}$	$7.22 \cdot 10^{-11}$
A_2	0.010	$6.87 \cdot 10^{-4}$	$1.00 \cdot 10^{-4}$	$-9.03 \cdot 10^{-8}$	$9.68 \cdot 10^{-11}$

The estimated thermal conductivity values are compared to the published values [3] in Fig. 11 for 400 K to 1500 K temperature range. TC location A_2, corresponding to the lowest z-value, provided the best comparison to the published values. The average relative difference between the thermal conductivity estimated from the A_2 TC location and published values was 5.4% over the entire temperature range. For temperatures above 800 K, the average relative difference was 2.3%. Again, the TC locations closer to the heat source deviated more from the published values.

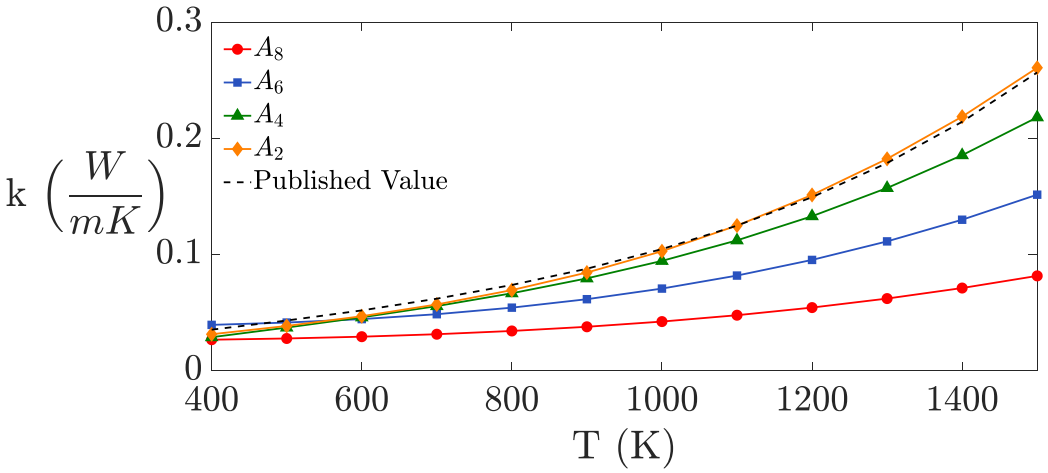

Figure 11. Thermal conductivity estimates from each TC location compared with published values at 1.33 kPa.

C. 13.33 Pa Thermal Conductivity Results

The temperature profile of the 13.33 Pa test is given in Fig. 12. The test consisted of six ramps and dwells ranging from 300 K to approximately 1750 K. The thermal conductivity was approximated between 300 K and 1700 K.

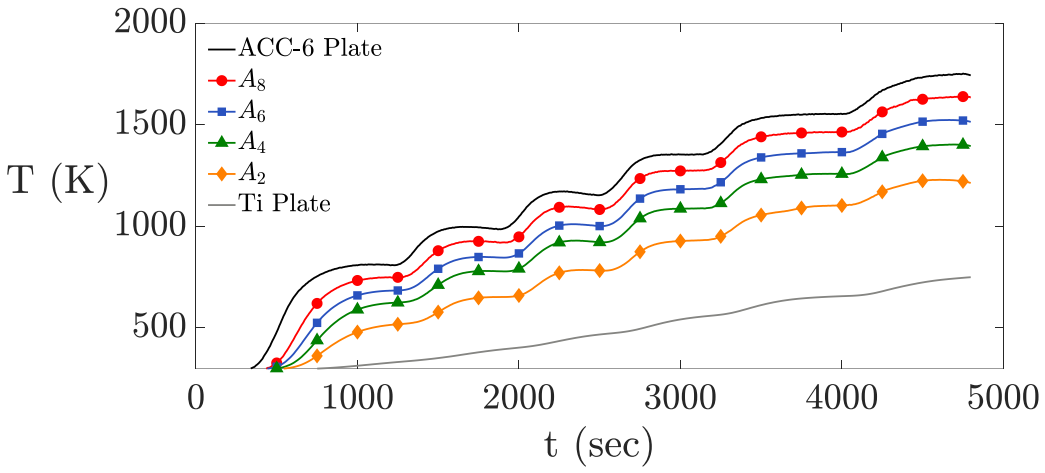

Figure 12. Temperature data collected from experimental apparatus at 13.33 Pa.

The algorithm searched for the coefficients of the thermal conductivity in Eq. 4 which minimized the objective function at each of the four TC locations, and the results are given in Table 3. TC location A_2 produced the largest *z*-value and A_4 produced the lowest *z*-value.

Table 3. Thermal conductivity coefficients and associated objective function values for each TC location at 13.33 Pa.

TC Location	z	c_0	c_1	c_2	c_3
A_8	0.274	$-5.88 \cdot 10^{-3}$	$2.67 \cdot 10^{-5}$	$-2.54 \cdot 10^{-9}$	$3.06 \cdot 10^{-11}$
A_6	0.124	$-1.89 \cdot 10^{-3}$	$1.70 \cdot 10^{-5}$	$-8.52 \cdot 10^{-9}$	$3.26 \cdot 10^{-11}$
A_4	0.067	$3.16 \cdot 10^{-3}$	$4.97 \cdot 10^{-6}$	$-1.55 \cdot 10^{-8}$	$6.67 \cdot 10^{-11}$
A_2	0.363	$5.92 \cdot 10^{-4}$	$2.60 \cdot 10^{-5}$	$-5.92 \cdot 10^{-8}$	$9.83 \cdot 10^{-11}$

The associated thermal conductivity results are compared with the published values [3] in Fig. 13 for 300 K to 1700 K. The A_4 solution gave the smallest percent difference when compared to the published values [3]. The average percent difference between the published and estimated values using the A_4 TC location was 9.44% over the entire temperature range. Above 800 K, the percent difference was 2.41%. TC location A_2 produced the largest *z*-value but had the second best solution compared to the published values. The TC locations closest to the heat source produced the estimates with the largest difference compared to the published values.

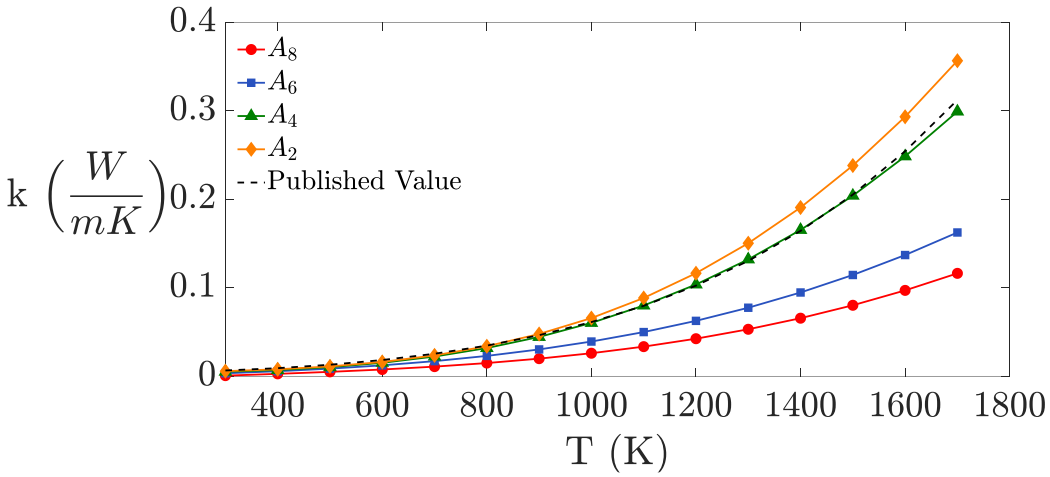

Figure 13. Thermal conductivity estimates from each TC location compared with published values at 13.33 Pa.

Unlike the previous results, TC location A_2 did not give the best solution when compared to the published values. However, the A_2 location z-value was extremely large compared to the A_4 z-value. Since the algorithm terminated because the maximum number of iterations were reached when estimating the coefficients at the A_2 location, a solution with a reduced z-value could result in a better estimate compared to the published data.

D. Specific Heat Results

The algorithm was applied to the 13.3 kPa temperature data discussed in the previous section to estimate specific heat. Specific heat does not vary with pressure for fibrous insulation, therefore the technique was only applied to test data at one pressure. The test was shorter in length, thus enabling fewer iterations and faster convergence of the solution. The resulting coefficients of Eq. 5 that minimized the temperature difference between the experimental data and numerical solution at the individual TC locations, Eq. 6, are given with their respective z-values in Table 4. The A_2 TC location produced the smallest z-value and A_6 produced the largest z-value.

Table 4. Specific heat coefficients and associated objective function values for each TC location at 13.3 kPa.

TC Location	z	b_0	b_1
A_8	0.123	$6.06 \cdot 10^3$	$8.09 \cdot 10^{-4}$
A_6	0.211	$1.81 \cdot 10^3$	$1.81 \cdot 10^{-3}$
A_2	0.021	$1.34 \cdot 10^3$	$2.81 \cdot 10^{-3}$

The specific heat results and published values [11] are compared in Fig. 14. The estimate from TC location A_2 had an average percent difference of 2.47% from the published values over the entire temperature range. TC location A_6 had the largest objective function value but was the second best estimate compared to the published values.

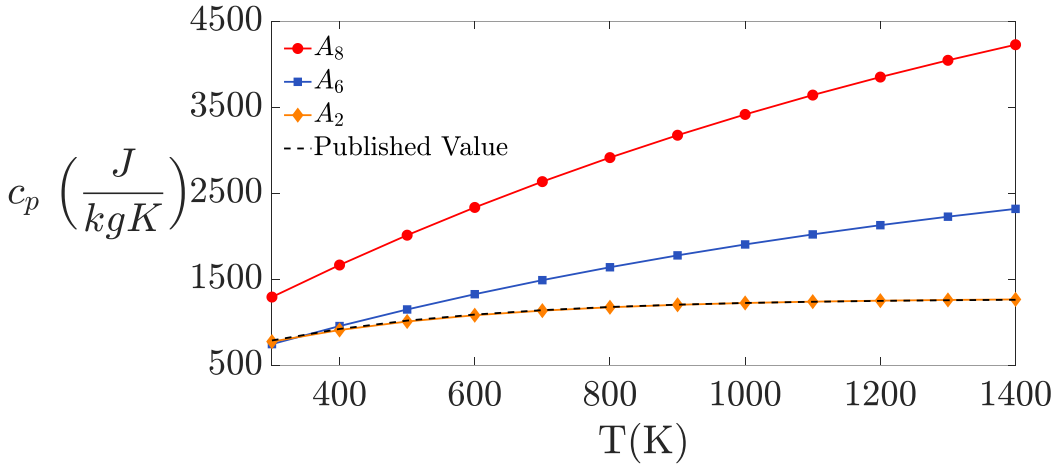

Figure 14. Specific heat estimates from each TC location compared with published values at 13.3 kPa.

VII. Analysis of Results

In the three sets of thermal conductivity results, the estimated values from the TC locations farthest away from the heat source, A_2 or A_4, gave the smallest percent difference from the published values. To better understand why the thermal properties were best approximated at the lower TCs, a sensitivity analysis of thermal conductivity with respect to location using the numerical model was performed for the 13.3 Pa test. To find the sensitivity of thermal conductivity with respect to location, the following partial derivative was approximated

$$\frac{\partial k}{\partial x} = \frac{\partial k}{\partial \hat{u}} \cdot \frac{\partial \hat{u}}{\partial x} \approx \left(c_1 + 2c_2\hat{u}(x) + 3c_3\hat{u}(x)^2\right)\left(\frac{\hat{u}(x+\Delta x)-\hat{u}(x)}{\Delta x}\right). \tag{7}$$

The partial derivative of thermal conductivity with respect to temperature, $\frac{\partial k}{\partial \hat{u}}$, was approximated using the functional representation of thermal conductivity, Eq. 4. The partial derivative of temperature with respect to location, $\frac{\partial \hat{u}}{\partial x}$, was approximated using a forward difference. The sensitivity of thermal conductivity with respect to location, Eq. 7, is shown in Fig. 15 for each TC location. During the initial two ramps of heating, thermal conductivity at the TC closest to the heat source, A_8, had the highest sensitivity. For the remaining 3000 seconds of the run, thermal conductivity at the TC location farthest away from the heat source had the highest sensitivity.

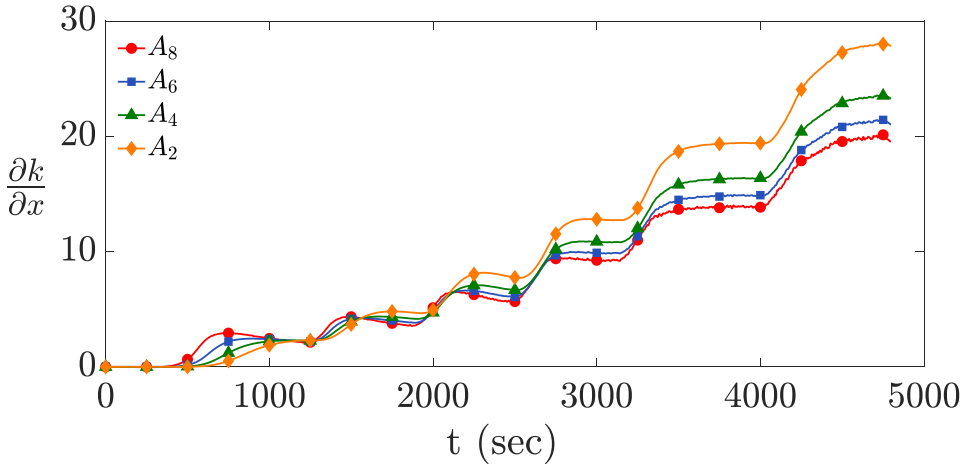

Figure 15. Sensitivity of thermal conductivity during experimental run with respect to location for the various TC locations.

The partial derivative approximations were evaluated using the 13.33 Pa test temperature data and the results of $\frac{\partial \hat{u}}{\partial x}$ and $\frac{\partial k}{\partial \hat{u}}$ at the four TC locations are shown in Fig. 16. The thermal gradient through the apparatus increased as time increased, resulting in larger $\frac{\partial \hat{u}}{\partial x}$ values for the locations farther from the heat source. The $\frac{\partial \hat{u}}{\partial x}$ values are larger than the $\frac{\partial k}{\partial \hat{u}}$ values, resulting in higher sensitivity at the locations farther from the heat source. Thus, a change in thermal conductivity, or coefficients of the functional form, at the locations farthest away from the heat source produced a larger change in the estimated temperature within the apparatus, therefore allowing the algorithm to better minimize the difference between the model and experimental temperature values.

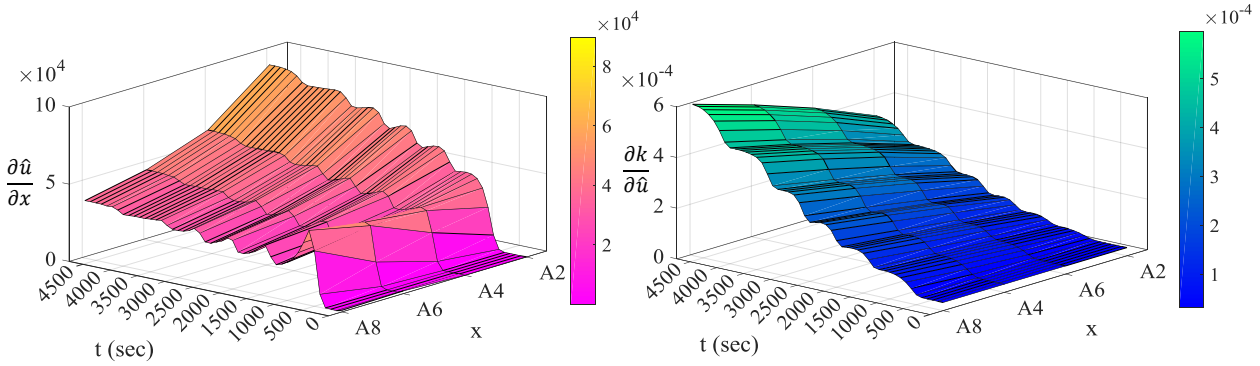

Figure 16. $\partial \hat{u}/\partial x$ and $\partial k/\partial \hat{u}$ approximations for the TC locations.

A thermal conductivity estimate from a TC location does not take the other locations through the APA into account. For example, thermal conductivity results at 13.3 kPa had two close z-values. TC location A_8 produced a *z*-value of 0.026 whereas A_2 produced a *z*-value of 0.023. The two thermal conductivity estimates varied greatly as the algorithm produced the results based on the TC location chosen for comparison to the temperature data in the objective function. The temperature values at the other TC locations were compared to the numerical model approximations at the corresponding locations to assess the impact of using a thermal conductivity estimate from one location. The relative temperature difference between the numerical approximation and the experimental data at location *j* is given by

$$\Delta T_j = \frac{|\hat{u}_j - A_j|}{A_j}, j \in \{2,4,6,8\}. \quad (8)$$

Using the 13.33 Pa temperature data, the temperature differences were found by solving for the numerical solution using the thermal conductivity estimates from each of the four TC locations and evaluating Eq. 8 at each location. The results are shown in Fig. 17. Recall for the 13.33 Pa test, A_4 provided the best results compared to the published values.

The temperature difference between the experimental data and numerical model at the TC location used to approximate the thermal conductivity was lower than the other locations as the algorithm attempted to minimize the difference at only that one location. For example, in Fig. 17c, the thermal conductivity estimate from TC location A_6 was used in the numerical model. The temperature difference between the experimental data and numerical model at the A_6 location was lower than the other locations. Shown in Fig. 17d, the temperature difference at the A_8 location was low because the A_8 thermal conductivity result was used. However, the temperature differences at the other locations were much larger compared to the other results using different thermal conductivity estimates. The overall temperature differences between the model and experimental values at all locations were lower when using the thermal conductivity solution obtained from the TC location A_4.

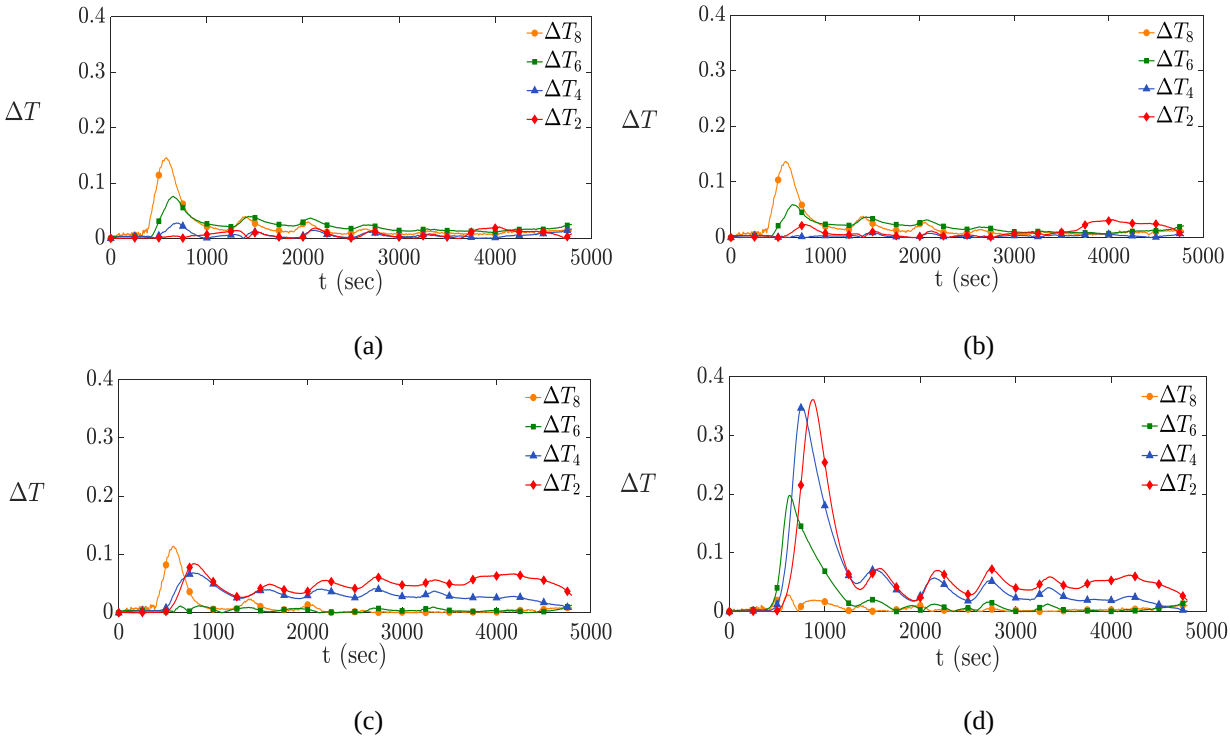

Figure 17. Temperature differences between experimental and numerical model values using thermal conductivity estimates from TC location: a) A_2, b) A_4, c) A_6, d) A_8.

VIII. Concluding Remarks

A methodology was developed to provide thermal property estimates of a fibrous insulation over the temperature range of 300 K to 1700 K, using transient temperature data. The temperature data was used in combination with a one-dimensional finite difference numerical model to replicate the heat conduction in the test assembly. The thermal property estimates were obtained by solving the inverse heat transfer problem using the CGA optimization technique to search the parameter space for coefficients of the functional representation of the thermal property. The algorithm used the possible coefficient solutions in the numeral model to estimate the temperatures within the setup. The numerical model temperature values at one TC location were then compared to the temperatures at the equivalent location within the experimental setup to determine the solution which minimized the objective function. The locations farthest away from the heat source provided the smallest percent difference between the estimated and published values for the specific temperature profiles used. The estimates were within 10% of known, published values over the entire temperature range and were within 3% of known, published values for temperatures larger than 800 K.

In the future, the methodology will be applied to other fibrous insulation materials with known thermal properties, analyzed in the same test assembly for further validation. The method will also be used to predict both thermal properties, i.e., thermal conductivity and specific heat, simultaneously. Of interest is evaluating the methodology for the test data with varied ramp style and rate as the temperature profile of the experimental transient data used had particular ramps and dwells. A change in the temperature profile is speculated to have an effect on the TC location that produces the best thermal property estimates compared to published values. Also of interest is the use of an objective function that incorporates the temperatures differences between model and data at all TC locations. Other changes such as a different objective function and manipulations to the search algorithm are desired to further study the methodology.

References

[1] ASTM C177-13, "Standard Test Method for Steady-State Heat Flux Measurements and Thermal Transmission Properties by Means of the Guarded-Hot-Plate Apparatus," ASTM International, West Conshohocken, PA, 2013, www.astm.org.

[2] ASTM C518-17, "Standard Test Method for Steady-State Thermal Transmission Properties by Means of the Heat Flow Meter Apparatus," ASTM International, West Conshohocken, PA, 2017, www.astm.org.
[3] Daryabeigi, K., Cunnington, G.R., and Knutson, J.R., "Combined Heat Transfer in High-Porosity High-Temperature Fibrous Insulation: Theory and Experimental Validation," *International Journal of Thermophysics*, Vol. 25, No. 4, October–December 2011, pp. 536-546.
[4] ASTM E1269-11, "Standard Test Method for Determining Specific Heat Capacity by Differential Scanning Calorimetry," ASTM International, West Conshohocken, PA, 2011, www.astm.org.
[5] Alifanov, O.M., and Mikhailov, V.V., "Solution of Nonlinear Inverse Thermal Conductivity Problem by the Iteration Method," *Journal of Engineering Physics*, Vol. 35, No. 6, Dec. 1978, pp. 1501–1506.
[6] Scott, E.P., and Beck, J.V., 1992, "Estimation of thermal properties in carbon/epoxy composite materials during curing," *Journal of Composite Materials*, Vol. 26, No. 1, pp. 20–36.
[7] Williams, S.D., and Curry, D.M., "Effective Thermal Conductivity Determination for Low-Density Insulating Materials," NASA TP-1155, Feb. 1978.
[8] Gosselin, A., Tye-Gingras, M., and Mathieu-Potvin, F., "Review of Utilization of Genetic Algorithms in Heat Transfer Problems," *International Journal of Heat and Mass Transfer*, Vol. 52, No. 9–10, April 2009, pp. 2169–2188.
[9] Hanuska, A.R., Scott, E. P., and Daryabeigi, K., "Thermal Characterization of Aerospace Structures," *Journal of Thermophysics and Heat Transfer*, Vol. 14, No. 3, July–September 2000.
[10] Garcia, S., Guynn, J., and Scott, E.P., "Use of Genetic Algorithms in Thermal Property Estimation: Part II—Simultaneous Estimation of Thermal Properties," *Numerical Heat Transfer*, Vol. 33, No. 2, 1998, pp. 149–168.
[11] Touloukian, Y.S., and Buyco, E.H., *Specific Heat-Nonmetallic Solids*, Thermophysical Properties of Matter, Volume 5, IFI/Plenum, New York, 1970.
[12] Blosser, M.L., Daryabeigi, K., Bird, R.K., and Knutson, J.R., "Transient Thermal Testing and Analysis of a Thermally Insulating Structural Sandwich Panel," NASA TM-2015-218701, March 2015.
[13] Thermophysical Properties Research Lab, "Thermophysical Properties of Ti-8-1-1 Alloy," TPRL Report #4677, March 2011.
[14] Bradie, B., *A Friendly Introduction to Numerical Analysis*, Pearson Prentice Hall, Upper Saddle River, 2006.
[15] Thomas, L.H., "Elliptic Problems in Linear Differential Equations over a Network," Watson Sci. Comput. Lab Report, New York, 1949, pp. 51-65.
[16] Haupt, R.L., and Haupt, S.E., *Practical Genetic Algorithms*, Wiley, Hoboken, 1998.
[17] Frye, E., "Thermal Property Estimation of Fibrous Insulation: Heat Transfer Modeling and the Continuous Genetic Algorithm," M.S. Thesis, Mathematical Sciences, Virginia Commonwealth Univ., 2018.